# Electronic Supplementary Information
# A method for extending AC susceptometry to long-timescale magnetic relaxation

Jeremy D. Hilgar, Aaron K. Butts, Jeffrey D. Rinehart*

Department of Chemistry and Biochemistry, University of California–San Diego, La Jolla, California 92093, United States. E-mail: jrinehart@ucsd.edu

## Contents

# 1 Preparative Details

## 1.1 General Considerations

Manipulations involving the synthesis of **1** were carried out in a nitrogen-atmosphere glovebox. Tetrahydrofuran (THF) and pentane were dried on activated alumina columns and stored over a 1:1 mixture of 3 and 4 Å molecular sieves. 1,6-heptadiyne (purchased from Alfa Aesar) was degassed using freeze-pump-thaw cycles prior to use. Nickel(II) bromide DME complex (Combi-Blocks), 18-crown-6 (18-c-6, Aldrich), anhydrous erbium trichloride (Aldrich), and potassium graphite ($KC_8$, Strem) were used as received. THF-$d_8$ was purchased from Sigma-Aldrich and was degassed using freeze-pump-thaw cycles, dried over stage 0 NaK on silica, and filtered before use. Neutral proligand hdcCOT was synthesized according to a literature procedure.[1] $^1$H NMR spectra were collected at –20 °C on a Jeol ECA 500 spectrometer. CHN elemental analysis was conducted by Midwest Microlab, Indianapolis, IN.

## 1.2 [K(18-c-6)][Er(hdcCOT)$_2$](1)

To a −50 °C stirring suspension of $KC_8$ (0.368 g, 2.72 mmol, 4 mL THF) was added a solution of hdcCOT (0.239 g, 1.30 mmol, 6 mL THF). The reaction mixture was allowed to warm to room temperature and was stirred for a total of 16 hours. Graphite was removed *via* centrifugation and subsequent filtration through a glass-fiber filter yielded a dark brown homogeneous solution. Concentration *in vacuo* and cooling to −50 °C yielded large yellow plates of $K_2$hdcCOT over the course of 24 hours. The mother liquor was removed from these plates and they were subsequently dried *in vacuo*; mass obtained: 0.261 g (Yield: 76.5%). $K_2$hdcCOT (0.182 g, 0.693 mmol) and $ErCl_3$ (0.095 g, 0.347 mmol) were combined in 20 mL THF and stirred for 16 hours. The resulting yellow suspension was centrifuged and the supernatant was separated and dried *in vacuo* to yield 0.149 g (74.7%) of K[Er(hdcCOT)$_2$] as a bright yellow powder. 18-crown-6 (0.0635 g, 0.240 mmol) was combined with this powder (0.1382 g, 0.240 mmol) in 20 mL THF and the resulting solution was stirred for 16 hours. Vapor diffusion of pentane into this solution yielded yellow rods of **1** (200 mg, Yield: 85.0%). CHN analysis (calculated, found) for $C_{40}H_{56}ErK$: C (57.25, 54.26); H (6.73, 6.51); N (0, 0).

# 2 Sample Characterization

## 2.1 $^1$H NMR of K[Er(hdcCOT)$_2$]

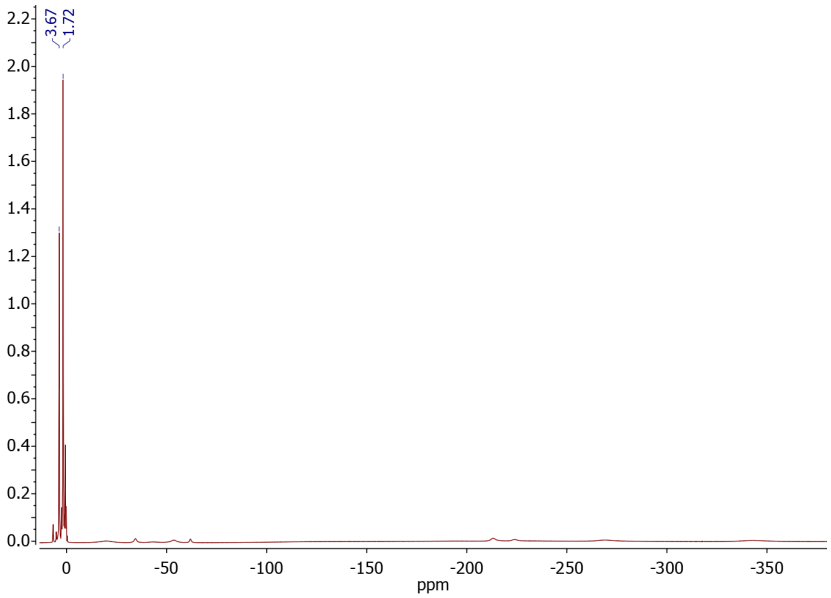


Figure S1: $^1$H NMR spectrum of K[Er(hdcCOT)$_2$] in THF-d$_8$ at –20 °C. Labelled signals correspond to THF residual peaks.

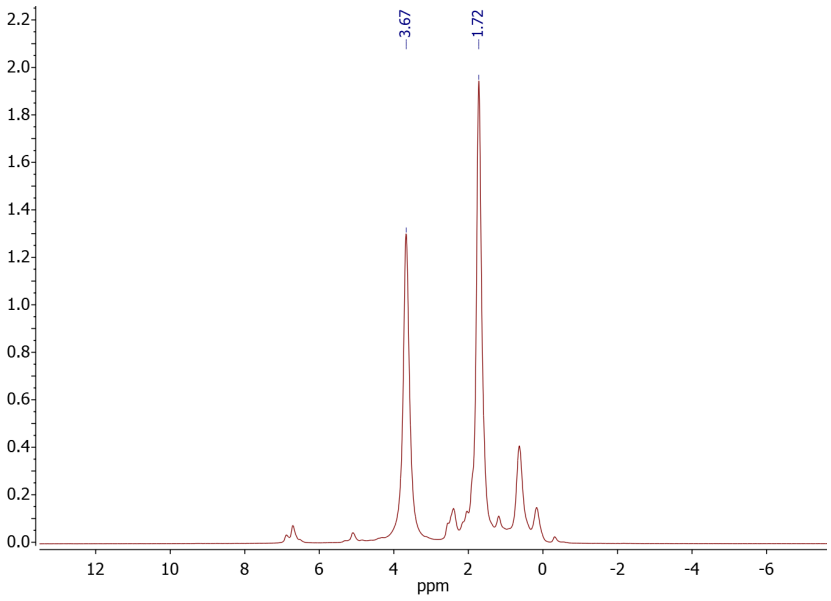


Figure S2: Downfield $^1$H NMR spectrum of K[Er(hdcCOT)$_2$] in THF-d$_8$ at –20 °C. Labelled signals correspond to THF residual peaks. Unlabelled signals are taken to be decomposition products.

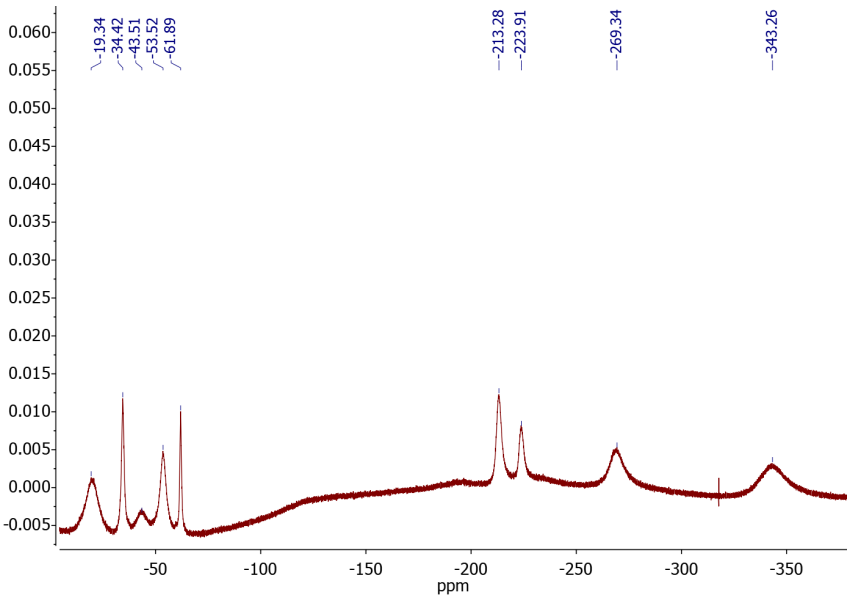


Figure S3: Upfield $^{1}$H NMR spectrum of K[Er(hdcCOT)$_2$] in THF-d$_8$ at –20 °C. Labelled signals correspond hdcCOT protons.

## 2.2 Crystallographic Methods

Single crystal diffraction data for **1** was collected at 100 K on a Bruker $\kappa$ Diffractometer using a Ga($K_\alpha$) METALJET source and a PHOTON II Area Detector. Data integration was carried out using SAINT and output intensities were corrected for Lorentz and air absorption effects. Additional absorption corrections were applied using SADABS. The structure was solved in space group No. 14 ($P2_1/n$) using direct methods with the SHELXT[2] program and anisotropic atom positions were refined against $F^2$ data using the SHELXL[3] program. Olex[2] was used during the refinement stage as a graphical front-end.[4] Real and imaginary anomalous dispersion coefficients for Ga($K_\alpha$) radiation were taken from the Brennan and Cowan[5] model. The position of all hydrogen atoms were determined using a riding model. Supplementary crystallographic data can be accessed from the Cambridge Crystallographic Data Center, CCDC 1939762.

## 2.3 Computational Details

*Ab initio* electronic structure modelling was carried out at the CASSCF level using the MOLCAS 8.2 software suite. Input atom coordinates were taken from crystallographic data and used without further geometry optimization. K, 18-c-6, and solvent THF were excluded from the input geometry. Basis functions of the ANO-RCC type were generated with the SEWARD module and the quality of a specific atomic basis function was determined as a function of the atom's distance from the $Er^{3+}$ ion (**Er:** ANO-RCC-VTZP; **atoms bound to Er:** ANO-RCC-VDZP; **all other atoms:** ANO-RCC-VDZ). To save disk space and reduce calculation cost two-electron integrals were Cholesky decomposed ($10^{-6}$ cutoff). A 7-orbital, 11-electron activate space (CAS(11,7)) was selected for the CASSCF calculation which was carried out with the RASSCF module. In this space all 35 configuration-interaction (CI) roots of spin multiplicity 4 and all 112 CI roots of spin multiplicity 2 were included. Spin-orbit matrix elements between CAS output wavefunctions were calculated with the RASSI module. SINGLE_ANISO was used to calculate relevant magnetic properties based on these multiconfigurational SCF results.

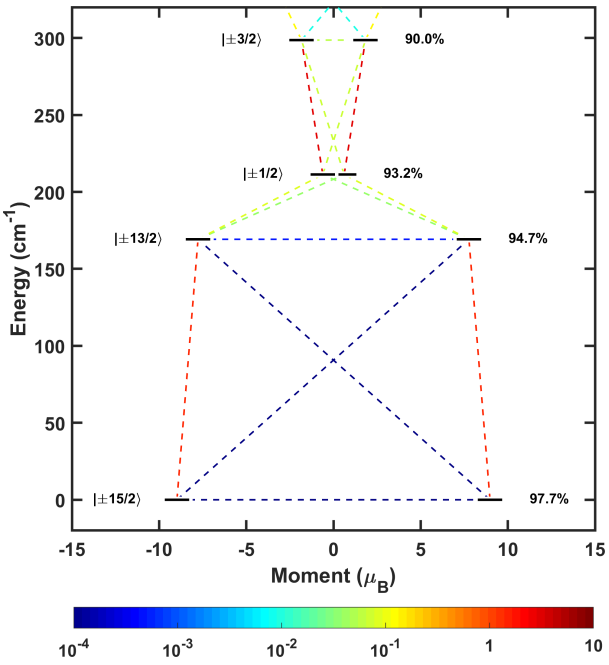


Figure S4: Calculated spectrum of the four lowest energy Kramers states for **1**. States (black lines) are labelled by their largest $\pm m_J$ component (left) and the percentage of that component (right). Transverse magnetic moment matrix elements (dotted lines) are colored according to their respective values (colorbar).

Table S1: $J = 15/2$ manifold energy spectrum of **1**.

| KD (i) | $M_z$ ($\mu_B$) | $E$ (cm$^{-1}$) |
|---|---|---|
| G | 8.976951952 | 0.000 |
| 1 | 7.769140677 | 169.229 |
| 2 | 0.613462182 | 211.322 |
| 3 | 1.834519491 | 298.637 |
| 4 | 6.547320548 | 411.560 |
| 5 | 3.031744486 | 433.319 |
| 6 | 4.722208148 | 542.787 |
| 7 | 5.730749227 | 550.231 |

Table S2: Selected average magnetic moment matrix elements between the $J = 15/2$ multiplets of **1**.

| KD (i) | $\langle i_\uparrow \vert \hat{M}_{avg} \vert i_\downarrow \rangle$ | $\langle i_\uparrow \vert \hat{M}_{avg} \vert i_\uparrow + 1 \rangle$ | $\langle i_\uparrow \vert \hat{M}_{avg} \vert i_\downarrow + 1 \rangle$ |
|---|---|---|---|
| G | 0.327451096777E-05 | 0.155011707285E+01 | 0.131694298009E-04 |
| 1 | 0.506016013299E-03 | 0.928060135350E-01 | 0.405995456082E-01 |
| 2 | 0.318682266522E+01 | 0.316661251988E+01 | 0.720938920092E-01 |
| 3 | 0.600396549586E-01 | 0.134946515237E+00 | 0.941722228670E-02 |
| 4 | 0.142404299502E-02 | 0.242852634761E+00 | 0.973779023853E-02 |
| 5 | 0.485270066726E-01 | 0.285000005858E+01 | 0.300470628704E-01 |
| 6 | 0.549287282880E-01 | 0.266558195629E+01 | 0.429984200984E-01 |
| 7 | 0.508798096471E-01 | | |

## 2.4 Magnetic Data Collection

Magnetic data were collected under DC scan and VSM scan modes using a Quantum Design MPMS 3 SQUID Magnetometer with equipped AC susceptibility attachment. Samples were loaded in custom quartz tubes (D&G Glassblowing Inc.) which were subsequently flame-sealed under static vacuum. To all samples was added a portion of melted eicosane wax to abate sample torquing and facilitate thermal conductivity. Diamagnetic contributions from the sample and eicosane were subtracted from all static moment data using Pascal's constants.[6] Magnetic relaxation data were collected in DC scan mode after first equilibrating the sample at a given temperature to a 7 T field then ramping the field (700 Oe $sec^{-1}$) to 0 T. Details related to the Fourier analysis of long-timescale magnetic data are discussed in the main text. MPMS3 data parsing, fitting, and plotting was performed with MATLAB; the object-oriented code package and documentation used for all processes is available at `https://www.github.com/RinehartGroup/qdsquid-dataplot`.

Table S3: Cole-Cole model fit values for standard AC data collected between 12–24 K.

| T (K) | $\chi_T$ (emu $mol^{-1}$) | $\chi_S$ (emu $mol^{-1}$) | $\alpha$ | $\tau$ (s) |
|---|---|---|---|---|
| 12 | 0.9326 | 0.065272 | 0.24752 | 1.0337 |
| 14 | 0.79015 | 0.056681 | 0.23844 | 0.10961 |
| 16 | 0.68433 | 0.051737 | 0.21928 | 0.017572 |
| 18 | 0.60431 | 0.049062 | 0.20683 | 0.004137 |
| 20 | 0.54347 | 0.050864 | 0.18359 | 0.0012833 |
| 22 | 0.49402 | 0.056917 | 0.15349 | 0.00049285 |
| 24 | 0.45171 | 0.085215 | 0.096429 | 0.00022233 |

Table S4: Cole-Cole model fit values for long-timescale AC data collected between 2–10 K.

| T (K) | $\chi_T$ (emu $mol^{-1}$) | $\chi_S$ (emu $mol^{-1}$) | $\alpha$ | $\tau$ (s) |
|---|---|---|---|---|
| 2 | 5.5958 | 0.93107 | 0.18269 | 53.716 |
| 4 | 2.9082 | 0.54772 | 0.17899 | 42.549 |
| 6 | 1.9509 | 0.40592 | 0.16944 | 37.459 |
| 8 | 1.3756 | 0.31299 | 0.15266 | 33.264 |
| 10 | 1.1006 | 0.37475 | 0.099677 | 13.494 |

$$\tau^{-1} = \tau_0^{-1} exp\left(\frac{-U_{eff}}{k_B T}\right) \tag{S1}$$

High-temperature relaxation mechanism equation. $\tau$ is the fitted relaxation time, $\tau_0$ is the attempt time, $U_{eff}$ is the effective barrier, $k_B$ is the Boltzmann constant, and $T$ is temperature.

$$\tau^{-1} = \tau_0^{-1} exp\left(\frac{-U_{eff}}{k_B T}\right) + \tau_{qtm}^{-1} + CT^2 \tag{S2}$$

General relaxation mechanism equation. $\tau$ is the fitted relaxation time, $\tau_0$ is the attempt time, $U_{eff}$ is the effective barrier, $k_B$ is the Boltzmann constant, $T$ is temperature, $\tau_{qtm}$ is the QTM relaxation time, and $C$ is the Raman relaxation coefficient. The Raman exponent was set to 2 for these fits, as this value gave consistently better agreement to the data over other integers.

Listing 1: Truncated MPMS3 MultiVu Sequence

```
Set Temperature 50K at 50K/min, Fast Settle
Wait For Temperature, Delay 0 sec, No Action

Magnet Reset
Wait For Delay 600 secs (10.0 mins), No Action

Set Temperature 2K at 50K/min. Fast Settle
Wait For Temperature, Delay 120 secs (2.0 mins), No Action

! REMARK - Frequency ~ 0.0264 Hz
MPMS3 Measure for 0.5 sec at 1 mm  every 0 sec Auto-Tracking
Wait For Delay 2 secs, No Action
Scan Time 0.0 secs in 20 steps
    Set Magnetic Field 8.00e at 30.000e/sec, Linear, Stable
    Wait For Field, Delay 15 secs, No Action
    Set Magnetic Field -8.00e at 30.000e/sec, Linear, Stable
    Wait For Field, Delay 15 secs, No Action
End Scan
Set Magnetic Field 0.00e at 30.000e/sec, Linear, Stable
Wait For Field, Delay 0 secs, No Action
Stop Measurements

Wait For Delay 60 secs (1.0 mins), No Action

! REMARK - Frequency ~ 0.0147 Hz
MPMS3 Measure for 0.5 sec at 1 mm  every 0 sec Auto-Tracking
Wait For Delay 2 secs, No Action
Scan Time 0.0 secs in 16 steps
    Set Magnetic Field 8.00e at 30.000e/sec, Linear, Stable
    Wait For Field, Delay 22 secs, No Action
    Set Magnetic Field -8.00e at 30.000e/sec, Linear, Stable
    Wait For Field, Delay 22 secs, No Action
End Scan
Set Magnetic Field 0.00e at 30.000e/sec, Linear, Stable
Wait For Field, Delay 0 secs, No Action
Stop Measurements

! REMARK - Frequencies truncated

Wait For Delay 240 secs (4.0 mins), No Action

! REMARK - Frequency ~ 0.00013 Hz
MPMS3 Measure for 0.5 sec at 1 mm  every 0 sec Auto-Tracking
Wait For Delay 2 secs, No Action
Set Magnetic Field 8.00e at 30.000e/sec, Linear, Stable
Wait For Field, Delay 3840 secs (1.1 hours), No Action
Set Magnetic Field -8.00e at 30.000e/sec, Linear, Stable
Wait For Field, Delay 3840 secs (1.1 hours), No Action
Set Magnetic Field 0.00e at 30.000e/sec, Linear, Stable
Wait For Field, Delay 0 secs, No Action
Stop Measurements

Set Temperature 300K at 50K/min. Fast Settle
Wait For Temperature, Delay 1 secs, No Action
```

Table S5: Fit values for relaxation mechanism parameters. Note these parameters are meant to highlight differences in the form of the relaxation data determined by different methods and are phenomenological.

| | $U_{eff}$ ($cm^{-1}$) | $\tau_0$ (s) | $\tau_{qtm}$ (s) | C ($K^{-2}s^{-1}$) |
|---|---|---|---|---|
| $\tau_{AC}$ | 147.7(7) | $3.1(1)\times10^{-8}$ | | |
| $\tau_{AC}+\tau_{VSM}$ | 142(3) | $4.7(1.0)\times10^{-8}$ | 54(7) | $2.2(8)\times10^{-4}$ |
| $\tau_{AC}+\tau_{str}$ | 146(5) | $3.5(1.1)\times10^{-8}$ | 141(31) | $6.2(6.2)\times10^{-5}$ |
| $\tau_{AC}+\tau_1$ | 154(13) | $1.8(1.0)\times10^{-8}$ | 1209(621) | $4.0(4.2)\times10^{-5}$ |
| $\tau_{AC}+\tau_2$ | 145(6) | $3.6(1.2)\times10^{-8}$ | 80(17) | $6.9(9.7)\times10^{-5}$ |

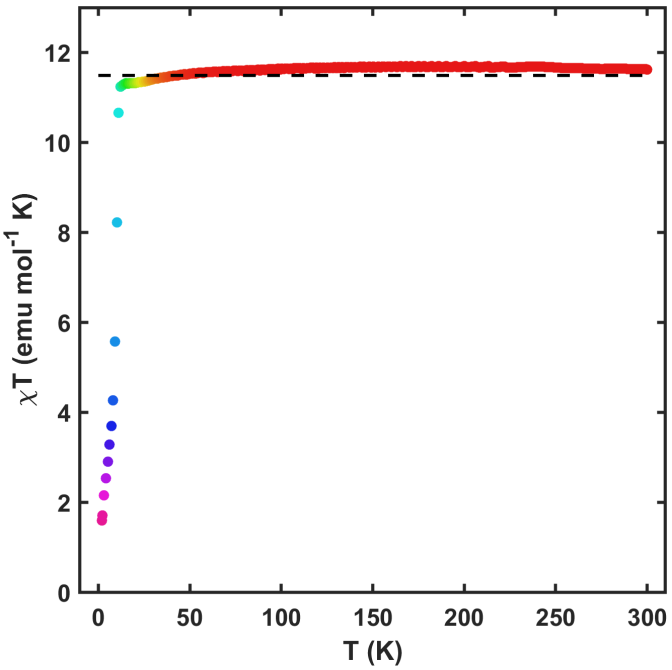


Figure S5: Magnetic susceptibility of **1** between 2 to 300 K. Colored dots are data measured under a 1000 Oe field and the dotted line is the theoretical $\chi T$ value for a free $Er^{3+}$ ion.

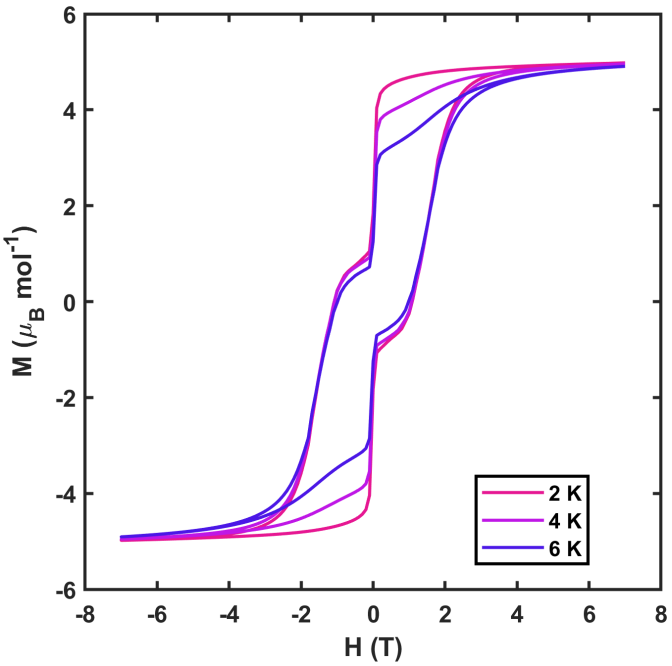


Figure S6: Isothermal magnetization of **1** from –7 to 7 T (Rate = 10 Oe sec$^{-1}$).

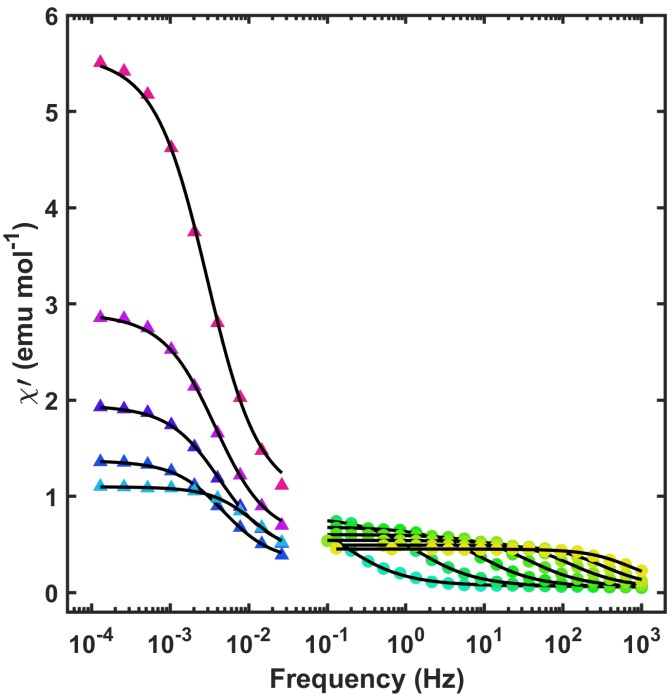


Figure S7: In-phase magnetic susceptibility of **1** bewteen 2 (fuschia) and 24 (yellow) K. Colored points are susceptibilities measured via standard AC measurements (circles) and extracted from Fourier analysis of VSM data (triangles). Black lines represent fits to a generalized Debye model (Equations 1 & 2).

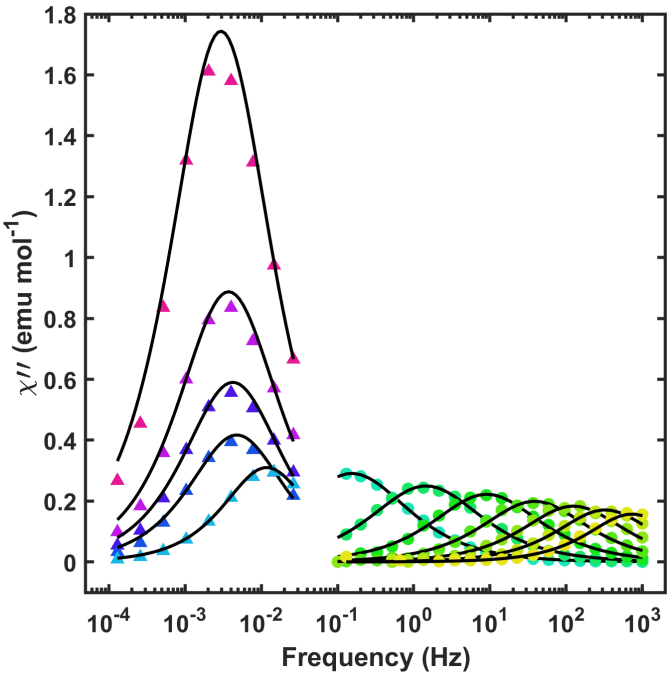


Figure S8: Out-of-phase magnetic susceptibility of **1** bewteen 2 (fuschia) and 24 (yellow) K. Colored points are susceptibilities measured via standard AC measurements (circles) and extracted from Fourier analysis of VSM data (triangles). Black lines represent fits a to generalized Debye model (Equations 1 & 2).

# References


[1] P. A. Wender and J. P. Christy, *Journal of the American Chemical Society*, 2007, **129**, 13402–13403.

[2] G. M. Sheldrick, *Acta Crystallographica Section A: Foundations and Advances*, 2015, **71**, 3–8.

[3] G. M. Sheldrick, *Acta Crystallographica Section C: Structural Chemistry*, 2015, **71**, 3–8.

[4] O. V. Dolomanov, L. J. Bourhis, R. J. Gildea, J. a. K. Howard and H. Puschmann, *Journal of Applied Crystallography*, 2009, **42**, 339–341.

[5] S. Brennan and P. L. Cowan, *Review of Scientific Instruments*, 1992, **63**, 850–853.

[6] G. A. Bain and J. F. Berry, *Journal of Chemical Education*, 2008, **85**, 532.